Towards Full Chamber HET Simulations with a Single 2D Hall Thruster Model

IEPC-2017-390

Lubos Brieda*
Particle In Cell Consulting LLC, Westlake Village, CA 91362

Michael Keidar
George Washington University, Washington, DC 20052

The work on modeling Hall thrusters has historically followed two independent paths. On one hand, codes were developed to model the plume of these devices. In parallel, other set of tools was developed to model the ionization and acceleration within the device. Combining these two sets of codes is not trivial due to the open geometry and operating principles of the Hall thruster. In this paper we review the legacy approach for Hall thruster modeling and demonstrate a new solver that captures the internal and external environments.

I. Introduction

Historically, the work on modeling Hall thrusters followed two distinct and for most parts, independent, paths. First, numerical tools were developed to model plumes of generic electric propulsion devices.[1–4] These "plume codes" generally utilize the Electrostatic Particle in Cell method (ES-PIC)[5] to self-consistently compute the expansion of ions from some given source. Many of these tools were originally developed to support ion thruster flight. In parallel, "device codes" were developed to model ionization and acceleration in the Hall thruster channel. Examples of these codes are the models of Fife[6] and Garrigues,[7] among others. These device codes also utilize the ES-PIC method, with a notable exception being the fully-fluid solver of Mikellides.[8] The primary difference between the plume and device codes is in the process used to compute plasma potential. In the device, the electron confinement by the magnetic field needs to be taken into account. Magnetic field effects are negligible in the plume.

As Hall thrusters replaced ion thrusters as the go-to technology for station keeping and orbit transfer, the need arose to also model their plumes. Plume simulations are useful, among other things, to study facility effects. Even the most efficient vacuum chambers will not achieve operating pressures comparable to the space environment. The plume of plasma devices can then be expected to artificially broaden due to an increased collisionality with neutrals. This effect is observed in ion thrusters as well. Unique to Hall thrusters is the mounting evidence from laboratory testing that discharge channel behavior is strongly affected by facility effects.[10] It is speculated that neutralized ions reflecting from a beam dump backstream into the device and artificially increase the local neutral population.

The open chamber design of Hall thrusters makes studying these devices challenging. Plume simulations require some set of initial conditions to define the plasma source. Since Hall thrusters are open to the ambient environment, there no longer exists a clear interface between the device and plume domain. Modern Hall thrusters are also designed to achieve majority of acceleration outside the device to minimize thruster channel erosion.[9] Plume simulations thus need to start at some downstream location to capture the full acceleration in the device, but this introduces its own complexities. Furthermore, numerically studying the effect of neutral ingestion requires a combined approach with bi-directional coupling. The legacy approach for modeling Hall thrusters is explored in the next section. There we attempt to summarize the challenges associated with the dual code approach. Next, a numerical model for a combined device-plume simulation is presented. This approach is demonstrated on simple test case. Finally the paper is concluded with a summary of future work.

*Contact email: lubos.brieda@particleincell.com

II. Review of Hall Thruster Modeling

The ES-PIC method used to model electric propulsion devices utilizes numerical "macroparticles" to simulate plasma constituents. Electrons are often treated as fluid, resulting in a hybrid scheme in which only the heavier ions and neutrals are modeled with particles. Each macroparticle represents some huge number (billions and often much more) of real particles since it is not numerically feasible to model every single ion or neutral for real-sized devices. Particle positions and velocities are updated from Newton's second law, $d\vec{x}/dt = \vec{v}$ and $d\vec{v}/dt = \vec{F}/m$. Generally only the Lorentz force, $\vec{F} = q(\vec{E} + \vec{v} \times \vec{B})$ is considered since gravitational effects are negligible at atomic scales. Magnetic field trapping is also negligible for the heavier ions, reducing the force term to the electrostatic $\vec{F} = q\vec{E}$. Ion and Hall thrusters operate at sufficiently low current densities where $d\vec{B}/dt = 0$ is valid, allowing one to compute the electric field from a scalar plasma potential, $\vec{E} = -\nabla\phi$. The major difference between plume and device codes then arises from the approach used to compute plasma potential.

A. Plume Codes

Starting with the electron momentum equation,

$$\frac{\partial}{\partial t}(m_e n_e \vec{v}_e) + m_e n_e (\vec{v}_e \cdot \nabla)\vec{v}_e = -en_e(\vec{E} + \vec{v} \times \vec{B}) - \nabla p_e + n_e m_e \nu(\vec{v}_i - \vec{v}_e) \tag{1}$$

we can eliminate the terms on the left hand side since electrons respond almost instantaneously to any disturbances, and $\partial/\partial t = 0$. The advective term is also small and can be ignored. Furthermore in the plume $B = 0$. Utilizing ideal gas law $p_e = n_e kT_e$, and letting $\vec{E} = -\nabla\phi$, we arrive at the reduced form

$$0 = \nabla\phi - \frac{k}{en_e}\nabla(n_e T_e) + \frac{1}{en_e}\vec{R} \tag{2}$$

where $\vec{R} = n_e m_e \nu(\vec{v}_i - \vec{v}_e)$ is the "friction term" arising from electron-ion collisions. Since $v_e >> v_i$, $v_i = 0$ can be assumed. Utilizing $\vec{j}_e = -en_e\vec{v}_e$, we write $\vec{R} = n_e m_e \nu \vec{j}_e/(en_e)$, giving us a generalized Ohm's law

$$0 = \nabla\phi - \frac{k}{en_e}\nabla(n_e T_e) + \frac{\vec{j}_e}{\sigma} \tag{3}$$

where $\sigma = (n_e e^2)/(\nu m_e)$ is the plasma conductivity.

Some additional simplifications can be made. First, in the limit $\nu \to 0$, the $\vec{R}$ term can be ignored and we have

$$\nabla\phi = \frac{kT_e}{en_e}\nabla n_e + \frac{k}{e}\nabla T_e \tag{4}$$

Next, assuming constant electron temperature, the second term disappears, and we obtain the famous Boltzmann relationship

$$n_e = n_0 \exp\left[\frac{e(\phi - \phi_0)}{kT_e}\right] \tag{5}$$

Here, ϕ_0 and n_0 are reference potential and plasma density sampled at the same spatial location. This is the model used in a vast majority of plume codes to represent the electron population. It is substituted into the Poisson's equation to give us the following expression for plasma potential:

$$\epsilon_0 \nabla^2\phi = e\left(n_i - n_0 \exp\left[\frac{e(\phi - \phi_0)}{kT_e}\right]\right) \tag{6}$$

Solving this equation numerically requires a mesh fine enough to resolve the local Debye length everywhere. This can prove problematic in the plume core where high plasma densities dictate the use of tiny cells. Instead, we assume quasineutrality, $n_e = n_i = n$, and invert Equation 5 to obtain a direct expression for potential,

$$\phi = \phi_0 + \frac{kT_e}{e}\ln\left(\frac{n}{n_0}\right) \tag{7}$$

This quasineutral approach offers an extremely rapid method to compute plasma potential in the plume but does not correctly resolve the potential drop in the non-neutral sheath. To address these challenges, a combined "Poisson switch" method was proposed by Santi.[11] With this scheme, the QN approach is used to first fix the potential in the dense plume, and then the Poisson's equation 6 backfills the low density region.

Instead of using constant temperature, electron temperature can be assumed to follow the polytropic relationship,

$$\frac{T_e}{T_{e,0}} = \left(\frac{n}{n_0}\right)^{\gamma-1} \tag{8}$$

This leads to an alternate form of the QN solver,[12]

$$\phi = \phi_0 + \frac{kT_{e,0}}{e}\frac{\gamma}{\gamma-1}\left[\left(\frac{n}{n_0}^{\gamma-1}\right)\right] \tag{9}$$

Unfortunately, both experimental work[13] and numerical analysis based on the fully kinetic approach[14] indicate that γ is not uniform everywhere.

To address these shortcoming, Boyd[15] proposed a detailed model for the near-field region of a Hall thruster. This model is based on retaining the friction term in the generalized Ohm's law,

$$\vec{j}_e = \sigma\left[-\nabla\phi + \frac{k}{en_e}\nabla(n_eT_e)\right] \tag{10}$$

and using charge conservation $\nabla\cdot\vec{j}=0$ to obtain an elliptic equation for ϕ. The model is coupled with mass conservation

$$\frac{\partial}{\partial t}(n_e) + \nabla\cdot(n_e\vec{v}_e) = n_en_aC_i \tag{11}$$

and energy conservation,

$$\frac{\partial}{\partial t}\left(\frac{3}{2}n_ekT_e\right) + \frac{3}{2}n_e\left(\vec{v}_e\cdot\nabla\right)kT_e + p_e\nabla\cdot\vec{v}_e = \nabla\cdot\kappa_e\nabla T_e + \vec{j}\cdot\vec{E} + 3\frac{m_e}{m_i}\nu_en_ek(T_e-T_H) - n_en_aC_i\epsilon_i \tag{12}$$

to obtain a self-consistent description of the electron fluid. Although showing promising results, this approach has historically not been widely utilized due to the added computational cost.

B. Device Modeling

On the other hand, device codes typically follow approach based on the thermalized potential model outlined by Morozov[16] and later implemented by Fife in HPHall.[6] In the Hall thruster, electrons are strongly coupled to the magnetic field lines. This allows the electron dynamics to be decomposed into motion along and perpendicular to a magnetic field line. In a magnetized plasma, $D_{e,\parallel} >> D_{e,\perp}$ anisotropy exists in the diffusion coefficient, and magnetic field lines become lines of constant temperature T_e and thermalized potential ϕ^*. We can write $T_e = T_e(\lambda)$, and $\phi^* = \phi^*(\lambda)$ where λ is a magnetic field line coordinate. Axisymmetry is implied by this formulation, since T_e and ϕ^* do not change with the azimuthal θ position.

The one-dimensional thermalized potential is related to the global plasma potential via

$$\phi^* = \phi - \frac{kT_e}{e}\ln(n_e) \tag{13}$$

From current conservation it is possible to derive an expression for the variation in ϕ^* with λ,

$$\frac{\partial\phi^*}{\partial\lambda} = \frac{-I_a + I_w - 2\pi k\frac{\partial T_e}{\partial\lambda}\int_0^l n_e\mu_{e,\perp}B(\ln(n_e)-1)r^2ds - 2\pi e\int_0^l n_iu_{i,\hat{n}}rds}{2\pi e\int_0^l n_e\mu_{e,\perp}Br^2ds} \tag{14}$$

Electron temperature is obtained from the energy equation,

$$\frac{\partial}{\partial t}\left(\frac{3}{2}n_ekT_e\right) + \nabla\cdot\left(\frac{3}{2}n_ekT_e\vec{u}_e + \vec{q}_e\right) + \nabla\cdot(n_ekT_e\vec{u}_e) = S_h - S_i \tag{15}$$

The major complexity in a Hall thruster code is in solving the above energy equation to obtain electron temperature as a function of λ. This involves capturing energy losses due to inelastic collisions with ions, Ohmic heating, and general thermal losses to the walls. However, once T_e is computed, ϕ^* can be easily obtained by integrating Equation 14. Then, the global two-dimensional ϕ is set from Equation 13. Electric field is obtained from $\vec{E} = -\nabla\phi$ and ion motion is integrated using the same set of equations used by plume codes. The energy equation is solved only within user-defined "anode" and "cathode" magnetic field lines, with approximation models used to set temperature upstream and downstream of these boundaries.

C. Device-Plume Coupling Challenges

Plume simulations require a set of initial conditions to define the plasma source. This involves specifying the mass flow rate and initial velocity distribution of the injected ions. Plasma potential on the injection surface also needs to be set. In the case of ion thrusters, there exists a clear interface between the device and plume environments. This is sketched in Figure 1(a). It is acceptable to start the plume simulation at the grids with ions injected from a Maxwellian distribution shifted by the potential drop across the ion optics. Any mass flow rate non-uniformities in the radial direction can be set based on Faraday probe measurements. A fixed potential can be applied on the grids, with this potential then used along with the local ion density to set the reference parameters for the Boltzmann relationship. With this approach we do not model the neutralizer cathode and the plume is assumed to be well mixed.

(a) Ion Thruster

(b) Hall Thruster

Figure 1. Comparison of the environment that needs to be considered for the ion and Hall thruster

Due to their open nature, Hall thrusters do not offer a comparable "exit plane" where the device physics ends and the plume simulation begins. This is sketched in Figure 1(b). While Hall thrusters have a physical exit plane, modern devices are designed to push much of acceleration outside the physical device to minimize wall erosion. Hall thrusters also exhibit various oscillations contributing to mass flow rate varying with time. Given that these devices are open to the ambient environment, it is conceivable that the downstream environment affects the actual behavior of the thruster itself.

Some of the earliest work on modeling Hall thruster plumes involved approach similar to ion thruster in which experimentally determined current densities were used to set the radial plume profile. Plume velocities were assumed to be Maxwellian and ions were injected at the physical thruster exit plane. Those models were not very successful in resolving all features of the plume. The next step in the evolution of device-plume coupling involved running the device code and sampling velocities and radial positions of ions crossing some pre-defined virtual plane to a file. This sampled data comprised a discretized velocity distribution function and could be used to generate particles for the plume simulation. Spicer[18] performed a detailed study of this coupling in his dissertation work. Figure 2 shows a typical result from his study. As can be seen, the results were mixed at best, with neither of the considered models fully capturing the experimental profile.

The coupling in those codes was clearly unidirectional. The device and plume simulations were run sequentially, with the prior producing initial conditions for the latter. Araki et.al.[4] expanded this approach by running both simulation codes concurrently, using MPI communication routines to transfer particles from HPHall to the plume simulation. Although that approach successfully captured the dynamic behavior of a Hall thruster discharge, the coupling still remained unidirectional. This is largely due to limitations of the device code. Although HPHall supports loading static background neutral density to correspond to chamber pressure, it doesn't contain functionality to inject neutrals from the downstream boundary to represent neutrals streaming from the chamber into the thruster channel.

Since much of acceleration in a Hall thruster happens outside the physical exit plane, it is necessary to sample ions at some downstream distance. In order to capture any possible charge exchange ions exiting at high angles, the sampling interface needs to be drawn to capture all possible exit trajectories. An arc

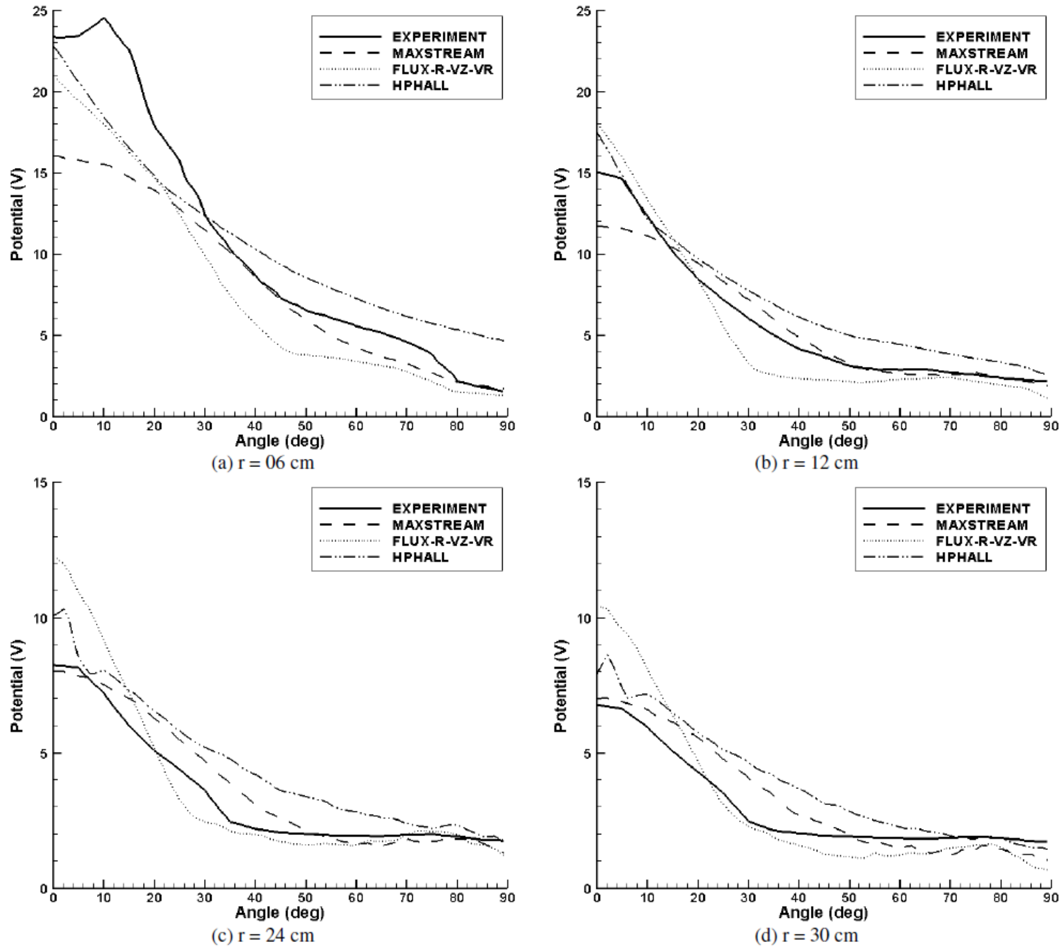

Figure 2. Figure from Ref.18, comparing several injection models for a Hall thruster plume simulation.

spanning the thruster axis and the physical thruster body is an acceptable option. This then results in the injection surface for the plume simulation in the shape of a hemisphere as illustrated in Figure 3. Such injection surface introduces a complication to the model which has yet to be satisfactory resolved. If the thruster is modeled in the plume simulation using the actual physical dimensions, the ion plume will originate from a region downstream of the thruster and a region void of plasma will exist between the thruster and the injection surface. A retarding electric field will develop along the injection interface as the simulation attempts to smooth out the non-physical gradient in charge density. The injected ions will be decelerated and the plume will not achieve the correct current density profiles. Attempts have been made to numerically set $E = 0$ in this "bubble", but these approaches were not completely successful. The alternative approach is to include the bubble with the thruster geometry giving the thruster a mushroom-like appearance. With this approach, a Dirichlet potential boundary condition can be set on the bubble surface using potentials computed by the device simulation. While this helps alleviate the formation of the retarding potential, it now becomes impossible to directly model any backflow of ions into the thruster channel, since the channel is no longer simulated. Furthermore, any slow moving charge exchange ions that would penetrate the near field region within the bubble will now be stopped by impacting the mushroom cap.

III. Two-Dimensional Hall Thruster Model

For this reason, we started exploring alternatives to the current dual code approach. The motivation for developing two sets of codes based on different numerical models was purely computational in nature. Ions and electrons follow the same set of fundamental laws of physics in both regions and hence a single

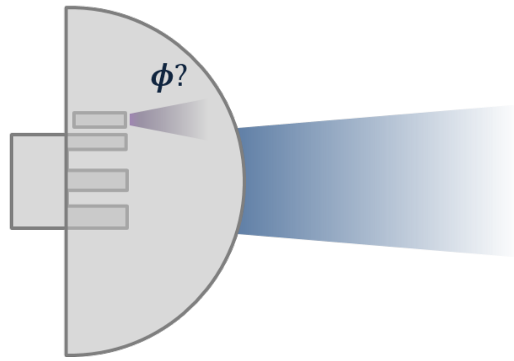

Figure 3. In order to capture external acceleration, ions need to be sampled downstream of the physical exit plane. This then results in the plume injection surface in the shape of a hemisphere.

solver should be capable of computing plasma potential in and outside the thruster. One such solver was recently demonstrated by Geng.[23] In that paper, we only focused on comparing the potential solution to one obtained assuming the thermalized model. Subsequently, the solver was implemented in our two-dimensional (Cartesian or axisymmetric) code for fluid dynamics, gas kinetics, and plasma physics called Starfish.[19] This code has been used for a wide range of problems, including modeling infiltration and removal of molecular contaminants from a purged cavity,[20] computation of conductance across a labyrinth vent,[21] and analyzing the impact of surface roughness on secondary electron emission.[22]

A. Solver Formulation

The electron momentum equation can be written as

$$\vec{j_e} = \mu\left(\vec{j_e}\times\vec{B}\right) + \sigma\vec{E} + \frac{\sigma}{en_e}\nabla p_e \tag{16}$$

where $\vec{j_e}$ is the electron current, p_e is the electron pressure, $\vec{B}$ is the magnetic field, $\sigma = \mu n_e e$ is the conductivity, m_e is the electron mass, and μ is the mobility. Using the ideal gas law, the pressure gradient is rewritten as $\nabla p_e = en_e\nabla T_e + eT_e\nabla n_e$. Here T_e is the electron temperature in eV units. With this substitution, electron current density is given by the following generalized Ohm's Law formulation:

$$\vec{j_e} = \mu(\vec{j_e}\times\vec{B}) + \sigma\vec{E} + \sigma(\nabla T_e + T_e\nabla\ln n) \tag{17}$$

This is the same equation used by Boyd in his detailed modeled with the additional $\vec{j_e}\times\vec{B}$ Hall term to capture magnetic confinement. This term naturally trends to zero as magnetic field weakens in the plume. Expanding this Hall term, a set of three equations can be obtained for components in the axial, radial, and azimuthal directions:

$$j_z = \mu(j_r B_\theta - j_\theta B_r) + \sigma E_z + \sigma(\nabla_z T_e + T_e\nabla_z\ln n) \tag{18}$$
$$j_r = \mu(j_\theta B_z - j_z B_\theta) + \sigma E_r + \sigma(\nabla_r T_e + T_e\nabla_r\ln n) \tag{19}$$
$$j_\theta = \mu(j_z B_r - j_r B_z) + \sigma E_\sigma + \sigma(\nabla_\theta T_e + T_e\nabla_\theta\ln n) \tag{20}$$

Due to axisymmetric geometry of the HT, the electric field and gradients of electron temperature and density are assumed to be zero in the azimuthal direction. It should be noted that this is a simplification in light of recent experiments demonstrating azimuthal spokes.[17] The azimuthal current density then reduces to $j_\theta = \mu(j_z B_r - j_r B_z)$ and can be substituted into Eqs. 18 and 19. This leads to the following set of coupled linear equations:

$$j_z = \mu\left[j_r B_\theta - \mu(j_z B_r - j_r B_z)B_r\right] + \sigma E_z + \sigma(\nabla_z T_e + T_e\nabla_z\ln n) \tag{21}$$
$$j_r = \mu\left[\mu(j_z B_r - j_r B_z)B_z - j_z B_\theta\right] + \sigma E_r + \sigma(\nabla_r T_e + T_e\nabla_r\ln n) \tag{22}$$

This system can be solved by matrix inversion to isolate the axial and radial component of the electron current density,

$$j_z = \mu_{11}\sigma(E_z + \nabla_z T_e + T_e \nabla_z \ln n) + \mu_{12}\sigma(E_r + \nabla_r T_e + T_e \nabla_r \ln n) \tag{23}$$
$$j_r = \mu_{21}\sigma(E_z + \nabla_z T_e + T_e \nabla_z \ln) + \mu_{22}\sigma(E_r + \nabla_r T_e + T_e \nabla_r \ln n) \tag{24}$$

where

$$\mu_{11} = \frac{1+\mu^2 B_z^2}{1+\mu^2 B^2}$$
$$\mu_{12} = \frac{\mu B_\theta + \mu^2 B_z B_r}{1+\mu^2 B^2}$$
$$\mu_{21} = \frac{-\mu B_\theta + \mu^2 B_z B_r}{1+\mu^2 B^2}$$
$$\mu_{22} = \frac{1+\mu^2 B_r^2}{1+\mu^2 B^2}$$

B. Mobility Models

While alternative methods have been used in the past to compute mobility,[24] here the analytical model consisting of classical elastic scattering from heavy particles (n) and Bohm diffusion (b) was used:

$$\mu_\perp = \alpha_n \frac{\mu_0}{1+(\omega_c/\nu_n)^2} + \alpha_b \frac{e}{m\nu_b} \tag{25}$$

where $\omega_c = eB/m_e$ and

$$\nu_n = n_n \sigma_{e,n} v_{e,th} \tag{26}$$
$$\nu_b = 16\omega_c \tag{27}$$
$$\tag{28}$$

Here $\sigma_{e,n}$ is the electron-neutral momentum transfer cross-section. The two α parameters are scaling coefficients useful in sensitivity studies.

C. Potential Solver

Defining $j = j_e - j_i$, total current density can be written as

$$j_z = Z_1 E_z + Z_2 E_r + Z_3 \tag{29}$$
$$j_r = R_1 E_z + R_2 E_r + R_3 \tag{30}$$

where

$$Z_1 = \mu_{11}\sigma \tag{31}$$
$$Z_2 = \mu_{12}\sigma \tag{32}$$
$$Z_3 = \mu_{11}\sigma\left(\nabla_z T_e + T_e \nabla_z \ln n\right) + \mu_{12}\sigma\left(\nabla_r T_e + T_e \nabla_r \ln n\right) - e n_i u_{i,z} \tag{33}$$
$$R_1 = \mu_{21}\sigma \tag{34}$$
$$R_2 = \mu_{22}\sigma \tag{35}$$
$$R_3 = \mu_{21}\sigma\left(\nabla_z T_e + T_e \nabla_z \ln n\right) + \mu_{22}\sigma\left(\nabla_r T_e + T_e \nabla_r \ln n\right) - e n_i u_{i,r} \tag{36}$$

Ion current is obtained from simulation particle densities and velocities. Using current conservation

$$\frac{\partial j}{\partial z} + \frac{\partial j}{\partial r} + \frac{j_r}{r} = 0 \tag{37}$$

we obtain

$$[Z_1^n E_z^n - Z_1^s E_z^s]\,\Delta r + [R_2^e E_r^e - R_2^w E_r^w]\,\Delta z = -S \tag{38}$$

where

$$\begin{aligned} S = &[(Z_2^e E_r^e + Z_3^e) - (Z_2^w E_r^w + Z_3^w)]\,\Delta r + \\ &[(R_1^n E_z^n + R_3^n) - (R_1^s E_z^s + R_3^s)]\,\Delta z + \\ &\frac{1}{r}\,[R_1 E_z + R_2 E_r + R_3]\,\Delta z \Delta r \end{aligned} \tag{39}$$

and n, s, e, and w are the values at the north, south, east, or west boundary of the node. Next, utilizing the electrostatic assumption allows us to write $\vec{E} = -\nabla\phi$. With the help of the standard finite difference formulation, Equation 38 can be rewritten as

$$\phi_{i,j} = \left[\frac{1}{(Z_1^e + Z_1^w)\Delta^2 r + (R_2^n + R_2^s)\Delta^2 z}\right] \tag{40}$$

$$\left[(Z_1^e \phi_{i+1,j} + Z_1^w \phi_{i-1,j})\Delta^2 r + (R_2^n \phi_{i,j+1} + R_2^s \phi_{i,j-1})\Delta^2 z + S\Delta z \Delta r\right] \tag{41}$$

D. Electron Temperature

A self-consistent temperature solver still remains as future work. In this paper we instead set the electron temperature axial profile to match experimental data presented in [25]. Magnetic field lines were assumed to be isothermal. Downstream of the magnetized region, a constant temperature model was used.

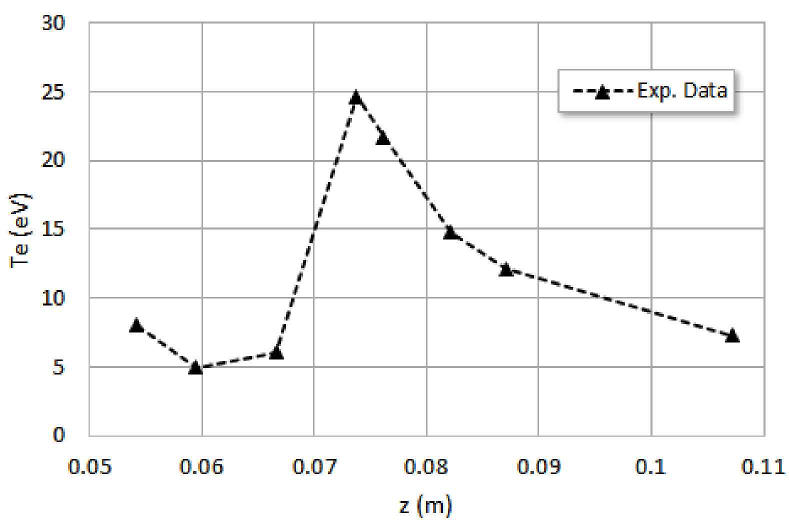

Figure 4. Electron temperature profile from [25]

IV. Simulation Setup and Preliminary Results

This two dimensional potential solver is demonstrated on a simple domain consisting of a Hall thruster placed in a vacuum chamber. The simulation domain is shown in Figure 5. These two plots show the computational mesh, with the first image showing a view zoomed in on the thruster channel. The magnetic field lambda mesh is also visible. This mesh is used by codes such as HPHall to compute potential. In our approach, it was merely used to fix electron temperature to follow the magnetic field lines. Only a single computational mesh with uniform mesh spacing was utilized. The mesh nodes colored red correspond to "internal" or Dirichlet nodes. The backflow region was not simulated and the thruster was modeled as if extending all the way to the chamber. This approach was taken due to some assumptions made originally in numerically implementing the Hall thruster potential solver from the previous section.

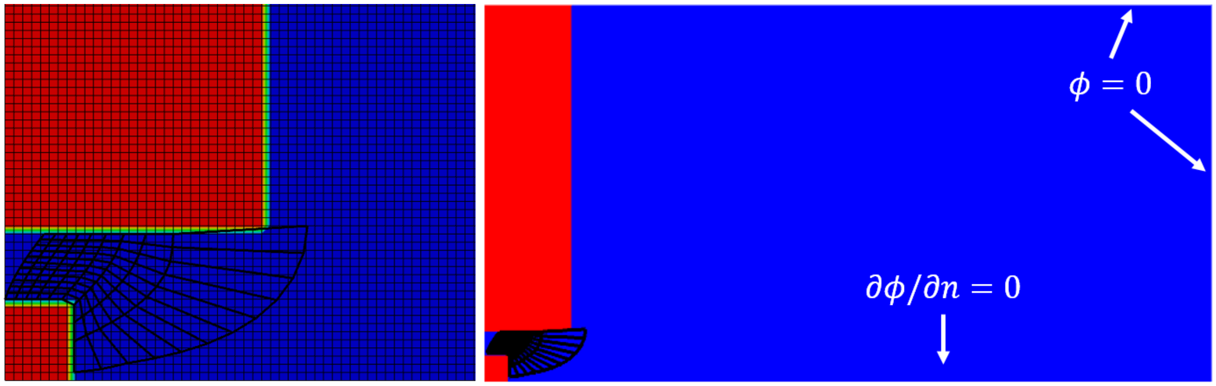

(a) Zoomed-in view (b) Full simulation domain

Figure 5. Simulation domain. Nodes colored in blue are the gas domain in which potential is solved.

A. Boundary Conditions

Boundary conditions need to be applied at several distinct regions: along thruster walls, the axis of symmetry, the anode, and at downstream. Along the walls, zero electric field was applied in the normal direction, $\partial\phi/\partial n = 0$. At the axis of symmetry, we have $\partial\phi/\partial r = 0$. Dirichlet boundary $\phi_{anode} = 300$V was applied at the anode. The downstream region corresponded to the vacuum chamber and $\phi = 0$V was set on the right and top boundary. Magnetic field lines were constructed from the stream function λ,

$$\frac{\partial\lambda}{\partial z} = rB_r$$
$$\frac{\partial\lambda}{\partial r} = -rB_z$$

Neutrals were injected at the anode. First-degree ionization was modeled as $\dot{n}_i = k(\theta)n_a n_e$, where the ionization rate is computed using the model of Fife as

$$k(\theta) = Q\beta_1\frac{I(\theta)}{\theta^{3/2}} \tag{42}$$

where $\theta = kT_e/\epsilon_i$, $u = \epsilon/\epsilon_i$, $Q = 4.13\times10^{-13}$ m^3/s, $\beta_1 = 1.00$, $\beta_2 = 0.80$ (for Xenon), and

$$I(\theta) = \int_1^\infty e^{-\frac{u}{\theta}}\frac{(u-1)}{u}\ln(1.25\beta_2 u)du \tag{43}$$

Creation of doubly-charged Xe^{++} ions was not considered in this work. Specific weight was set such that the simulation contained approximately 300,000 neutrals and 5.2 million ions at steady state. Simulation time step was set to 10^{-8} s and the simulation ran for 4000 time steps.

B. Preliminary Results

Preliminary results obtained on this mesh with the prescribed electron temperature are shown in Figure 6. These plots show the progression of plasma density (top) and potential (bottom). While the solution is not yet self-consistent due to the applied electron temperature, these results appear promising. Initially, the solution exhibits some transient numerical instabilities. However, once the channel fills with ions, the solver predicts a reasonable potential drop in the channel, with the potential drop appearing to closely follow the prescribed temperature profile. At a later time, the thruster discharge becomes steady and the solution shows a well defined plume. No subsequent breathing mode oscillations were observed but this could be due to the relatively short real time simulated here. The simulation spanned only a single breathing mode oscillation. These oscillations are due to variations in the production rate of ions, and their presence is not contingent on the choice of potential solver.

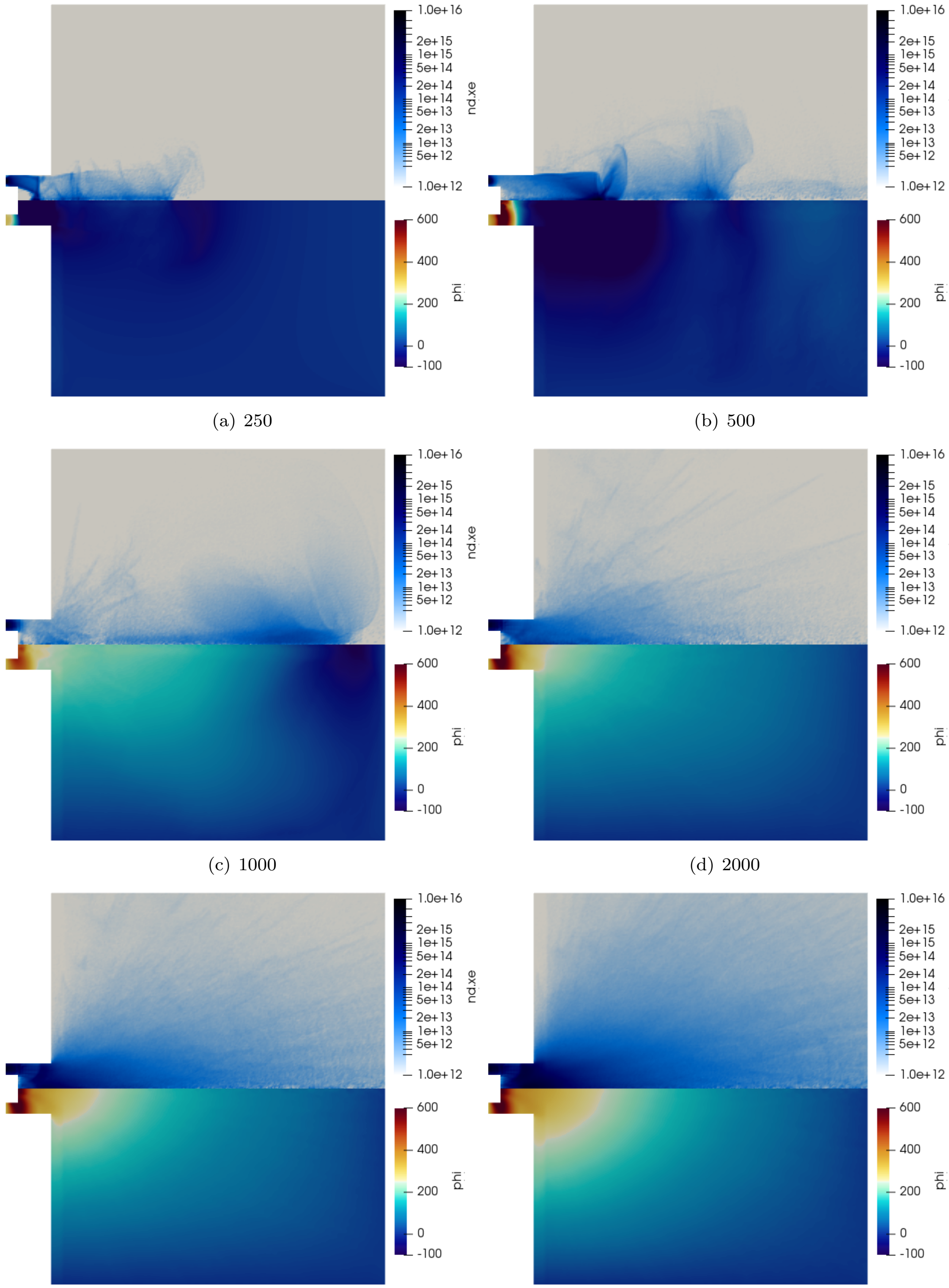

(a) 250 (b) 500

(c) 1000 (d) 2000

(e) 3000 (f) 4000

Figure 6. Preliminary results from the two-dimensional potential solver at various time steps. Temperature profile was set to experimental data and did not change during the simulation.

V. Conclusion and Future Work

In this work we described and demonstrated a two-dimensional potential solver that could be used to model both the device and plume environments of a Hall thruster. Historically, these two environments have been modeled with different sets of codes with different operating assumptions and coupling between them has proven difficult. A unified code could help alleviate the coupling challenges, and could be used to study effects such as facility effects where bi-directional coupling is important.

The code algorithm described here is not yet self-consistent, however. Specifically, the code is missing an electron temperature solver. In this work, electron temperature was set using experimental data. This solver will be implemented in the near future. Subsequently, the code will be utilized to study the effect of facility effects on thruster behavior.

References

[1] Samanta Roy, R. I., *Numerical Simulation of Ion Thruster Plume Backflow for Spacecraft Contamination Assessment*, Ph.D. thesis, Massachusetts Institute of Technology, 1995.

[2] Wang, J., Brinza, D., and Young, M., "Three-Dimensional Particle Simulations of Ion Propulsion Plasma Environment for Deep Space 1," *Journal of Spacecraft and Rockets*, Vol. 38, 2001, pp. 433–440.

[3] Brieda, L., *Development of the Draco ES-PIC Code and Fully-Kinetic Simulation of Ion Beam Neutralization*, Master's thesis, Virginia Tech, 2005.

[4] Araki, S. J., Martin, R. M., Bilyeuy, D., and Koo, J., "SM/MURF: Current Capabilities and Verification as a Replacement of AFRL Plume Simulation Tool COLISEUM," *52nd AIAA Propulsion and Energy Forum*, Salt Lake City, UT, 2016.

[5] Birdsall, C. and Langdon, A., *Plasma physics via computer simulation*, Institute of Physics Publishing, 2000.

[6] Fife, J. M., *Hybrid-PIC Modeling and Electrostatic Probe Survey of Hall Thrusters*, Ph.D. thesis, Massachusetts Institute of Technology, 1998.

[7] Garrigues, L., Hagelaar, G. J. M., Boeuf, J. P., Raitses, Y., Smirnov, A., and Fisch, N. J., "Two Dimensional Hybrid Model of a Miniaturized Cylindrical Hall Thruster," *30th International Electric Propulsion Conference*, Florence, Italy, 2007, IEPC-2007-157.

[8] Mikellides, I. G. and Katz, I., "Numerical simulations of Hall-effect plasma accelerators on a magnetic-field-aligned mesh," *Physical Review E*, Vol. 86, No. 046703, 2012.

[9] Hofer, Richard, R., Goebel, D. M., Mikellides, I. G., and Katz, I., "Magnetic shielding of a laboratory Hall thruster. II. Experiments," *Journal of Applied Physics*, Vol. 115, No. 043304, 2014.

[10] Walker, M. L. R., *Effects of Facility Backpressure on the Performance and Plume of a Hall Thruster*, Ph.D. thesis, University of Michigan, 2005.

[11] Santi, M. M., *Hall Thruster Plume Simulation Using a Hybrid-PIC Algorithm*, Master's thesis, 2013.

[12] Boyd, I. and Dressler, R. A., "Far field modeling of the plasma plume of a Hall thruster," *Journal of Applied Physics*, Vol. 92, No. 4, 2002.

[13] Nakles, M., Brieda, L., Reed, G. D., Hargus, W. A., and Spicer, R., "Experimental and Numerical Examination of the BHT-200 Hall Thruster Plume," *43rd AIAA Joint Propulsion Conference*, Cincinnati, OH, 2007, AIAA-2007-5305.

[14] Hu, Y. and Wang, J., "Modeling Electron Characteristics in an Ion Thruster Plume: Fully Kinetic PIC vs. Hybrid PIC," *35th International Electric Propulsion Conference*, Atlanta, GA, 2017.

[15] Boyd, I. and Yim, J. T., "Modeling of the near field plume of a Hall thruster," *Journal of Applied Physics*, Vol. 95, No. 9, 2004.

[16] Morozov, A. I., Esinchuk, Y. V., Tilinin, G. N., Trofimov, A., Sharov, Y. A., and Shchepkin, G. Y., "Plasma accelerator with closed electron drift and extended acceleration zone," *Soviet Physics – Technical Physics*, Vol. 17, No. 1, 1972.

[17] Ellison, C., Raitses, Y., and Fisch, N., "Cross-field electron transport induced by a rotating spoke in a cylindrical Hall thruster," *Physics of Plasmas*, Vol. 19, No. 1, 2012, pp. 013503.

[18] Spicer, R., *Validation of the DRACO Particle-in-Cell Code using Busek 200W Hall Thruster Experimental Data*, Master's thesis, Virginia Polytechnic Institute and State University, 2007.

[19] Brieda, L. and Keidar, M., "Development of the Starfish Plasma Simulation Code and Update on Multiscale Modeling of Hall Thrusters," *48th AIAA Joint Propulsion Conference*, Atlanta, GA, 2012.

[20] Brieda, L., Newcome, J., and Errigo, T., "Diffusion of Water into Purged Volumes," *SPIE Optics & Photonics Conference*, San Diego, CA, 2014.

[21] Brieda, L. and Gordon, T., "Analysis of molecular conductance through a labyrinth vent," *SPIE Optics & Photonics Conference*, San Diego, CA, 2014.

[22] Rose, L. P., *Development of 1D Particle-in-Cell Code and Simulation of Plasma-Wall Interactions*, Master's thesis, George Washington University, 2014.

[23] Geng, J., Brieda, L., and Michael, K., "On applicability of the "thermalized potential" solver in simulations of the plasma flow in Hall thrusters," *Journal of Applied Physics*, Vol. 114, No. 103305, 2013.

[24] Brieda, L., *Multiscale Modeling of Hall Thrusters*, Ph.D. thesis, The George Washington University, 2012.

[25] Raitses, Y., Smirnov, A., and Fisch, N. J., "Effects of enhanced cathode electron emission on Hall thruster operation," *Physics of Plasmas*, Vol. 16, No. 05716, 2009.